The Design of a New Solar-powered Unmanned Aircraft

Li Songqi, Yu Tianning, Wang xuchen, Li Haoran

Northwestern Polytechnical University, Xi'an, P.R.China

1 Introduction

1.1 Introduction of solar-powered unmanned aircraft

Solar-powered aircraft is based on solar radiation as its propulsion. As an ideal air flight platform, solar-powered aircraft uses solar energy as the energy source, which helps avoid the burden of traditional airborne fuel and realize the long voyage,. It can replace the interrupted communication in various natural disasters; it can fly over the Typhoon, tracking and detecting the storm; it can also can hover and scout the enemy in a predetermined airspace for long time, guiding aircraft targets. So it has broad application prospects in both military and commercial fields.

1.2 Development of solar-powered unmanned aircraft

At the end of the 70's, development of human plane help accumulate the experience of manufacturing low speed, low wing loading, and light weight aircrafts. On this basis, in the early 80's, American developed the "solar Challenger" - a single-seat solar powered aircraft. The plane has a wingspan of 14.3 meters, wing loading of 60 KPa, empty weight of 90 kg, and a total of 16128 pieces of silicon solar cell on the wing and horizontal tail surfaces. It has an output power of 3000 watts or more of the ideal sunlight. In July, 1981, the plane successfully flew from Paris to the British, with an average speed of 54 km, and a range of 290 km.

People put forward a kind of high-altitude, low-speed, remote controlled solar-powered unmanned aircraft. The solar radiation during the day is used to climb (or to store in the battery), at night, it glides on the high altitude (or obtain energy from the battery). Use the inexhaustible solar energy, it can maintain a long flight. This kind of aircrafts can be used for meteorological observation and reconnaissance missions first.

1.3 Main work of this paper

Using solar energy as power source, using high efficiency, light weight, lithium ion polymer battery as storage equipment, using large torque DC motor to drive, using high efficiency propeller propulsion, we design a vertical takeoff and landing

unmanned aircraft, which includes: the overall design, the aerodynamic design, and the power system design.

2 Overall Design of the Unmanned Solar-powered Aircraft

2.1 Fundamentals of the unmanned solar-powered aircraft

The aircraft collect with solar energy solar panels, and through the Maximum Power Point Tracker (MPPT), a part of the energy will be stored in the battery, the other part is for the need of energy to drive the parts on the airplane, as shown above, the steering gear motor, airborne equipment, etc.; At night, the airplane only relies only on the energy stored in the battery to maintain the flight.

2.2 Description of the missions

Unmanned solar-powered aircrafts are mainly used for reconnaissance, surveillance, image information collection and other tasks, generally equipped with cameras, thermal imaging equipment etc.. The missions are shown in Figure 2-1.

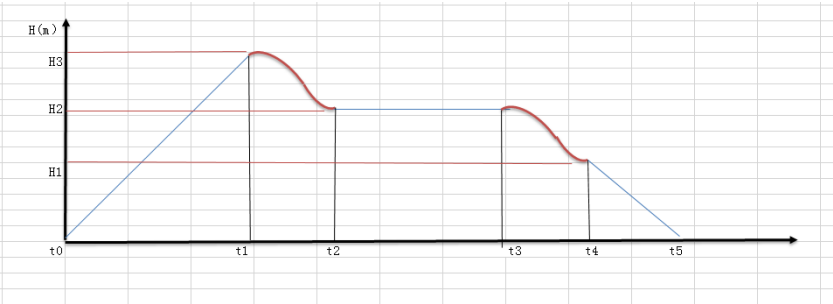

Figure 2-1 The Missions of Unmanned Solar-powered Aircrafts

The first stage (t0-t1): the maximum tension force to climb (approximately uniform velocity)

The second stage (t1-t4): cruise with the constant power (t1-t2; t3-t4 are too short to take into consideration)

The third stage (t4-t5): uniform descent and landing

By remote controller, solar electric propulsion system boots the aircraft and makes it takeoff vertically on the ground without a runway. After reaching the predetermined height of about 300 meters, the aircraft operated by remote controller

goes down to the task level and starts the cruise flight to begin scheduled tasks. After the mission is finished, it changes to vertical descent flight, and lands slowly.

In the mission above:

(1) Vertical takeoff demands a tension greater than the sum of the aircraft weight, the load and the resistance.

(2) Solar-powered aircraft requires a reasonable layout of solar panels and sufficient power to supply for motor propeller and other power facilities.

In order to design an unmanned solar-powered aircraft system, a fully consideration of plans, mission equipment, power systems, portability, take-off and landing should be put forward in the task-oriented design of the aircraft platform layout.

2.3 Vertical take-Off and landing (VTOL) implementation

VTOL unmanned aircrafts with small sizes require less power and low flight speed. Thus, the power devices are mostly small power turbine shafts or piston engines, some adopt the turbofan engines as well. The power system determines the most VTOL unmanned aircrafts are rotor aircrafts. According to the way to create thrust (pull), rotor aircrafts which currently has VTOL capability is divided into two categories: directional thrust and reversing thrust.

2.4 Select the overall layout of the aircraft

The main purpose of this subject is to use solar energy as power source, with high efficiency, light weight of lithium ion polymer battery as storage equipment, with large torque DC motor to drive, with high efficiency propeller in the propulsion system, designing solar unmanned aircraft that can VTOL. The overall layout of the aircraft must be able to meet the requirements, of which the main is to adopt a vertical take-off and landing layout.。

We adopt the conventional layout (of which the technology is mature, the design and manufacture process is easy), high span chord ratio (a necessary condition to realize the solar powered aircraft), and reversing thrust tilt wing type. Its advantage is that (a) the wings can be adjusted to the proper angle of attack in order to keep the level flying state while tilt rotors achieve reversing thrust, (b) the structure is simple. To achieve such layout, three sets of power plant are needed, two large power motor propeller should be installed on both sides of the symmetrical wing, and a small power motor propeller should be installed in the center of the horizontal tail for the balance of the aircraft. The layout diagram is as follows:

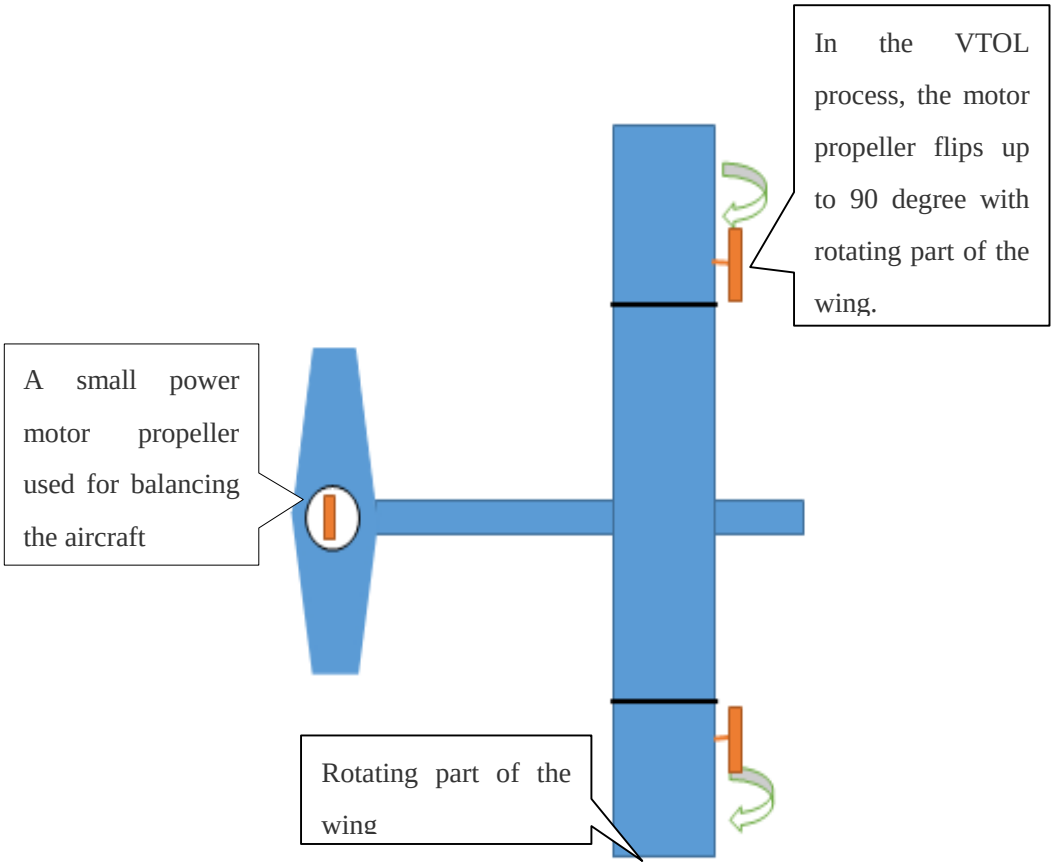

Fig. 2-2 layout of the aircraft

3 Detailed 3D Aircraft layout design based on UG

3.1 Research on power and energy systems design

Solar-powered aircrafts need to collect and store enough energy during the day in order to provide the energy for day and night flight. Such energy is provided by the solar cells or storage batteries installed on its wings. The power system of solar powered aircraft is the key to the structural design. The power system consists of solar cells and storage batteries, electric motors, a propeller, energy control and management system. If characteristics of these components change, the size of the aircraft will be impacted.

3.1.1 Solar panel selection

The power of solar powered aircrafts is driven completely from energy produced by the solar cell. Taking into account the cost of production, the extent of application and degree of maturity, we choose monocrystalline silicon solar cells. It has the density of 0.4kg/m^2, and its photoelectric conversion efficiency is about 13% - 18%, and can reach 20% experimentally.

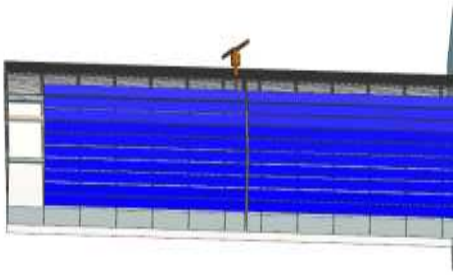

Fig. 3-1 arrangement of solar cells

3.1.2 Storage battery selection

The secondary power supply is the onboard energy storage device. It should have high efficiency of charge and discharge ability and high energy density. Taking into account the cost of production, the extent of application and degree of maturity of the technology, we choose lithium ion batteries. Because we design small model aircraft

unmanned aerial vehicle (UAV), so the high energy density of the fuel cell is not suitable. On the other hand, the energy density of the lithium battery is about 110-170Wh/kg, specific power is 1000-1200W/kg, which meets the requirements of our design.

3.1.3 Motor selection

In this paper, permanent magnet brushless rare earth motor is chosen. Our design requirements are: the plane is less than 6 kg weight, load in 2 kg, with maximum 8 kg weight in calculation. The propeller motor we selected must be able to lift such a weight in the process of VTOL. In the general plane layout design, we choose two high power rotor providing the main traction motor with propeller, and the other small motor only serve to balance the plane. So each powerful propeller must provide at least 4 kg tension. According to the above requirements, we select 2 QA-5308-350KV motors and a general motor.

Fig. 3-2 QA-5308-350KV motor

3.1.4 Propeller selection

When the aircraft is in climbing, acceleration and level cruising, we must ensure that the aircraft will be able to overcome the wind resistance, air temperature and air density, the environmental conditions, etc. Generally aircraft driven by propellers use variable pitch propellers to adjust the power. But recently foreign researchers use fixed pitch propeller, setting the pitch to the best place before the plane reach the cruising altitude. The variation of the motor speed can make up for the deficiency in other high pitches. We choose the fixed pitch propellers in our design, which can greatly reduce the weight of the structure.

By looking for information and adapting with the maximum power of the motor above, we choose GEMFAN electric propeller 16 * 8: 16 inch diameter, 8 inches pitch (400mm) and 50 grams weight.

Fig. 3-3 GEMFAN 16X8 propeller

We choose a small power motor with a common folding propeller. Its blade radius is about 100mm and serve as a balance propeller.

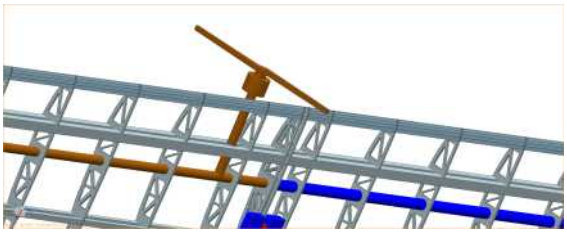

Fig. 3-4 distribution of the motor and propellers

Fig. 3-5 the two high power rotor propeller

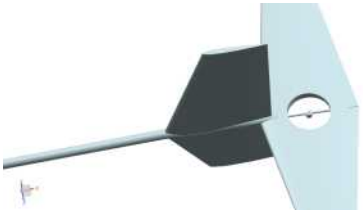

Fig. 3-6 balancing propeller of the flat tail

3.2 UAV take-off weight estimation

Solar-powered UAV takeoff weight can be calculated from the following formula:

$$m_{total} = m_{structure} + m_{propulsion} + m_{battery} + m_{load} \quad (3\text{-}1)$$

m_{total}: aircraft take-off weight，which is a constant during the flight; $m_{structure}$: aircraft structural weight; $m_{propulsion}$: propulsion system weight; $m_{battery}$: aircraft battery weight, including the weight of solar panels and storage batteries; m_{load}: the weight of load.

(1) The structural weight：

$$m_{structure} = \alpha_1 m_{total} \quad (3\text{-}2)$$

α_1: the structural weight coefficient, in our calculation α_1=0.25; m_{total}: total weight of the aircraft.

Fig. 3-7 wing ribs designation

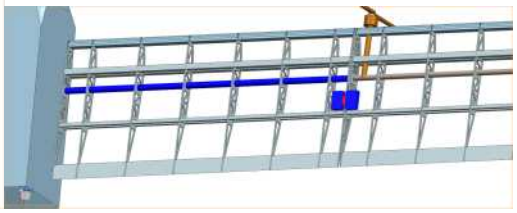

Fig. 3-8 the wing structure

Fig. 3-9 skin design

(2) The propulsion system weight

The total weight of the propulsion system satisfies the following f ormula

$$m_{propulsion} = m_{motor} + m_{reducer} + m_{speeder} + m_{propeller} + m_{steering} + m_{bolter} + m_{worm} + m_{other} \quad (3\text{-}3)$$

In our calculation:

$$m_{total} = 370g + 100g + 130g + 90g + 40g + 200g + 150g + 120g = 1.2kg$$

(3) The power battery weight

$$m_{battery} = m_{storagebattery} + m_{batterypanel} = 2.53kg \quad (3\text{-}4)$$

(4) load： $m_{load} = 2kg$

According to the above analysis, the aircraft takeoff weight can be expressed as:

$$m_{total} = \frac{m_{power} + m_{battery} + m_{load}}{1 - \alpha_1} \quad (3\text{-}5)$$

$m_{power}=1.2kg$； $m_{battery}=2.53kg$； $m_{load}=2kg$； $\alpha_1=0.25$. Take these data into (3-8）we can calculate: $m_{total}=7.64kg$, which meets the design requirements.

3.3 Airfoil profile and rotating wings layout

3.3.1 Airfoil profile selection

In the existing airfoil profile data (from the Profili software)，we compare the lift-drag ratio and choose the most reasonable airfoil shape. Several airfoils which have the relatively large lift-drag ratio are listed below:

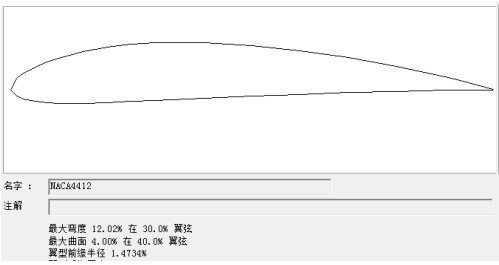

Fig. 3-10 NACA4412 airfoil

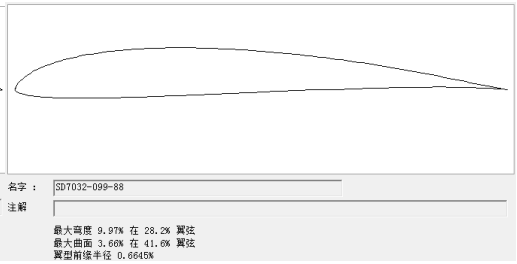

Fig. 3-11 SD7032-099-88 airfoil

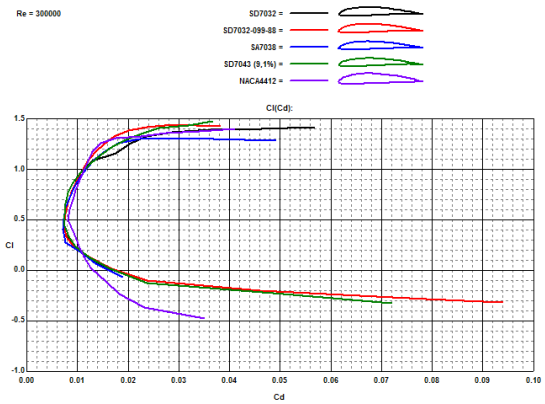

Fig. 3-12 Cl-Cd curves of 5 airfoils when Re=300000

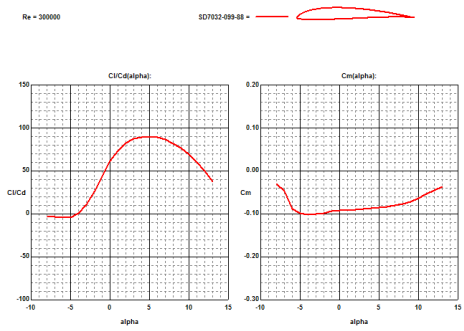

Fig. 3-13 the lift-drag ratio of SD7032-099-88 when Re= 300000

SD7032-099-88 - Re = 300000				
Alfa	Cl	Cd	Cl/Cd	Cm
-4.0	0.0159	0.0167	0.9521	-0.1014
-3.0	0.1289	0.0122	10.5656	-0.1003
-2.0	0.2362	0.0092	25.6739	-0.0990
-1.0	0.3347	0.0078	42.9103	-0.0945
0.0	0.4479	0.0073	61.3562	-0.0926
1.0	0.5567	0.0076	73.2500	-0.0916
2.0	0.6640	0.0081	81.9753	-0.0903
3.0	0.7694	0.0088	87.4318	-0.0890
4.0	0.8720	0.0098	88.9796	-0.0873
5.0	0.9731	0.0108	90.1019	-0.0855
6.0	1.0706	0.0120	89.2167	-0.0833
7.0	1.1627	0.0135	86.1259	-0.0805
8.0	1.2481	0.0153	81.5752	-0.0767
9.0	1.3260	0.0173	76.6474	-0.0720
10.0	1.3805	0.0201	68.6816	-0.0640
11.0	1.4178	0.0237	59.8228	-0.0545

Fig. 3-14 the aerodynamic parameters of SD7032-099-88when Re= 300000

Compared from the data above， we finally choose SD7032-099-88.

3.3.2 Determine the parameters

We choose the straight wing and the chord length $b = 550mm$.

Designed flight conditions are listed below:

Cruise altitude: $h = 200m$

Cruise speed: $V = 8m/s$;

Chord length: $b = 550mm$;

Flight Reynolds number: $\mathrm{Re} = 296520 \approx 300000$;

Stagger angle $\alpha = 3°$

Airfoil length $l = 5266mm$

Aspect ratio $\lambda = 9.57$

Total area $S = 2.8961m^2$

After calculation, we can get:

Lift coefficient $C_Y = 0.6148$

Resistance coefficient $C_{Xtotal} = 0.0214$

3.3.3 Rotating wings layout

In order to achieve vertical take-off and landing of the aircraft, we choose rotating wing layout. Because differential of the two propellers in the ends of the wings can achieve steering, there are no the ailerons or flaps. Problems in the design process are as follows:

(1) The size of rotating wings

If the rotating wing part accounted for a too large proportion of the whole wing, it will be more difficult to achieve rotation during the flight process and the rotation resistance will be relatively large. According to the information we know: rotating parts should be 40% of the wing span at best, which are 1050mm on both sides.

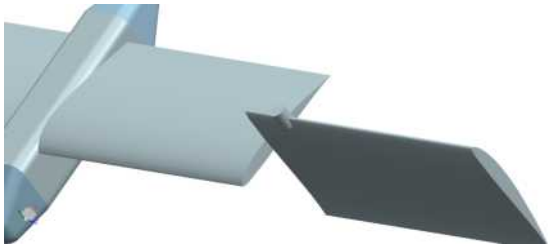

Fig. 3-15 layout of the rotating wing

(2) Realization of the rotating wings

Rotating parts of the wings should be driven by a motor and rotate through the gear set. So the position of the rotating axis should be chosen in the axis through the center of gravity, thus rotating wings wouldn't be unsteady or difficult to control because of imbalance. At the same time, as the plane is a large aspect ratio aircraft, we choose the worm wheel and worm to realize rotating wings, as shown in Figure 3-17.

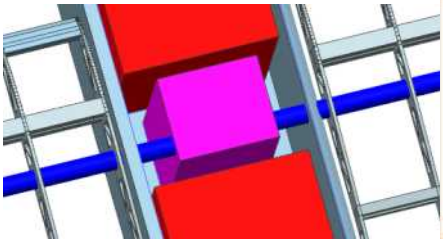

Fig. 3-16 worm gear

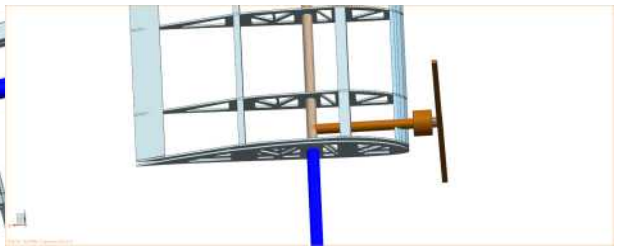

Fig. 3-17 rotating part of the wing

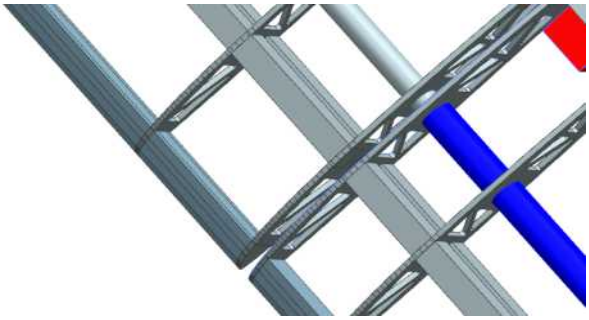

Fig. 3-18 connection of the rotating part

When the aircraft turns its direction from perpendicular to level, rotating parts of the wings need to be level. In order to ensure stability during the level flight, electronic bolts should be installed between the rotating wings and the fixed wings, preventing relative rotation caused by resistance, improving the stability of the flight.

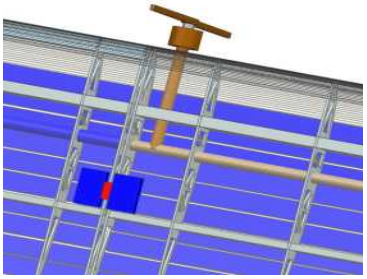

Fig. 3-19 electronic bolts

3.4 Design of the fuselage and wings

3.4.1 Size of the fuselage

In general, the length of the fuselage should be 60% of the span length, which is $L = 5.266m \times 60\% \approx 3.2\,\mathrm{m}$ in our design.

3.4.2 Horizon tails and rudder design

Airfoil profile selection

Horizontal tails and vertical tail are all symmetrical airfoils. From the former experience, we choose NACA0009 airfoil in the Profili database.

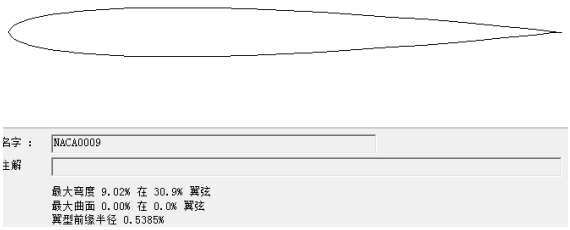

Fig. 3-20 NACA0009airfoil

The main function of the horizon tail is to balance the longitudinal moment caused by wings, the torque efficiency they can provide is proportional to the lift and the moment arm, and the lift is proportional to its area. Therefore, tail efficiency is proportional to the product of its tail area and the moment arm, which is:

$$A_H = \frac{L_H S_H}{b_a S_W} \qquad (3\text{-}6)$$

L_H： moment arm of the horizon tail; b_a： Average aerodynamic chord length, which is chord length in our aircraft. S_H: Exposed area of the horizon tail; S_W: total area of the wing.

We choose the isosceles trapezoid horizontal tails; $S_H = 20\%, S_W = 0.579m^2$, root shoot ratio=2; then the span of the horizon tail $l = 1520mm$； chord length at the root=508mm，chord length at the shoot=254mm; moment arm of the tail $L_H = 2221mm$; proportion of the elevator at the tail in the tail string is 25%.

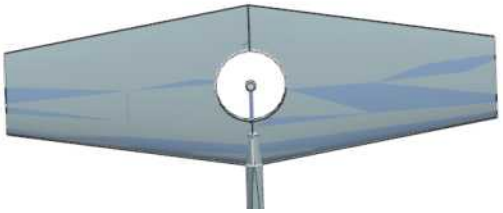

Fig. 3-21 horizon tail

3.4.3 Vertical tails and rudder design

Vertical tail efficiency is proportional to the product of its tail area and the moment arm, which is:

$$A_V = \frac{L_V S_V}{l S_W} \qquad (3\text{-}7)$$

L_v：moment arm of the vertical tail; S_V: Exposed area of the vertical tail; S_W: total area of the wing.

We choose the right angled trapezoid vertical tails; $S_V = 16\% S_W = 0.46m^2$； then the span of the vertical tail $l = 1025mm$； chord length at the root=550mm，chord length at the shoot=330mm; moment arm of the tail $L_V = 1540mm$; proportion of the elevator at the tail in the tail string is 20%.

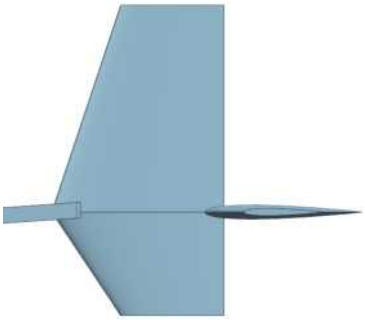

Fig. 3-22 vertical tail

We design a vertical tail extending 365mm downward from the tail of the aircraft, which help solve the landing problem and enhance the flight stability.

4 Numerical simulation and the aerodynamic analysis

4.1 Grid generation

In order to reduce the number of grid without affecting the quality of the mesh, we use a combination of structured meshes and unstructured meshes to generate a flow field computational grid. The aircraft is wrapped inside a moderate size volume flow field, of which the internal grids are unstructured, the external grids are structured. The aircraft surface and the flow field have a total of 1616397 hybrid grids.

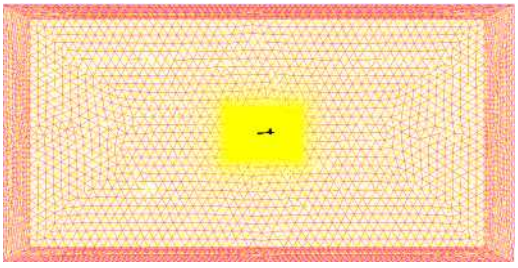

Fig. 4-1 mesh of the aircraft and the outer flow field

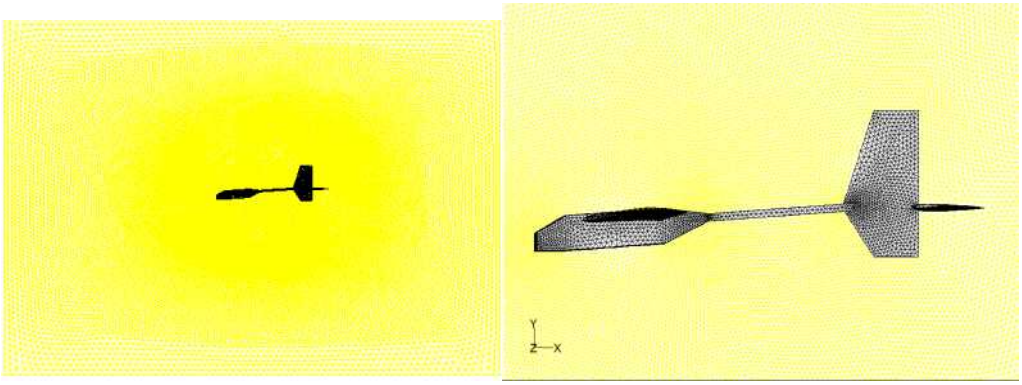

(a) (b)

Fig. 4-2 mesh of the aircraft

4.2 Results of numerical calculation and aerodynamic analysis

We set up nine calculation targets in this calculation. The only variety in these calculations is the angle of attack (4 °, - 2 °, 0 °, 2°, 4 °, 6 °, 8 °, 10 ° and 12 °).

Boundary conditions:

Speed: $V = 8m/s$, $Ma = 0.024$;

Pressure: $P = 97940Pa$;

Temperature: $T = 287.6K$;

(1) Calculating results

We choose four groups of operating modes for analysis (4 °, 0 °, 6 ° and 12 °)

4.3.1 Pressure distribution

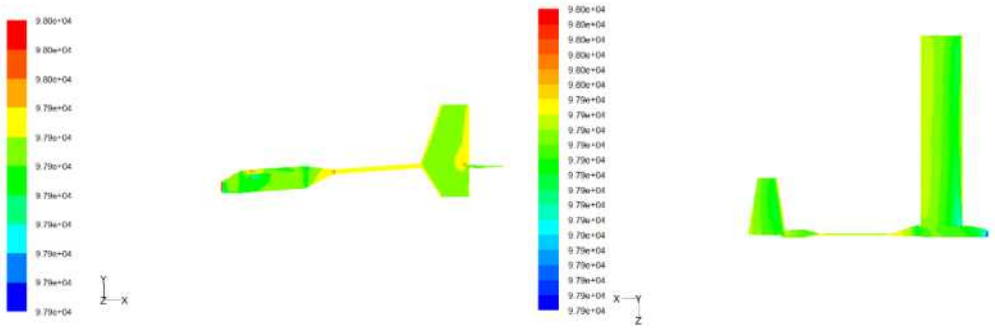

(a) (b)

Fig. 4-3 pressure distribution of the plane surface at -4° angle of attack

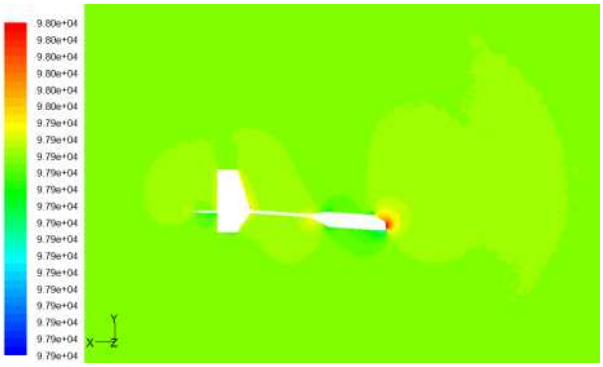

Fig. 4-4 pressure distribution at -4° angle of attack

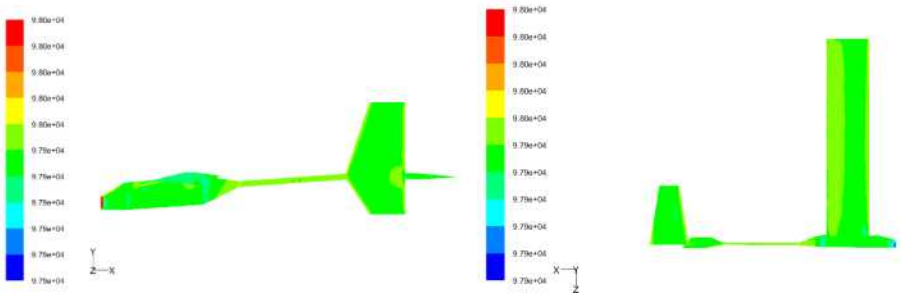

(a) (b)

Fig. 4-5 pressure distribution of the plane surface at 0° angle of attack

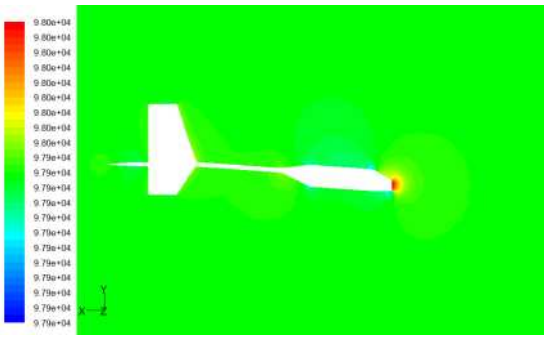

Fig. 4-6 pressure distribution at 0° angle of attack

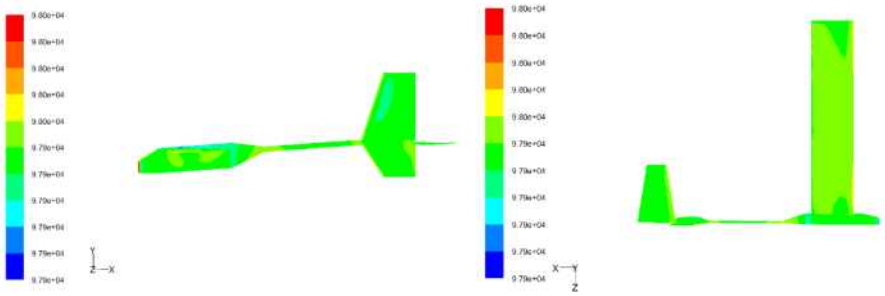

(a) (b)

Fig. 4-7 pressure distribution of the plane surface at 4° angle of attack

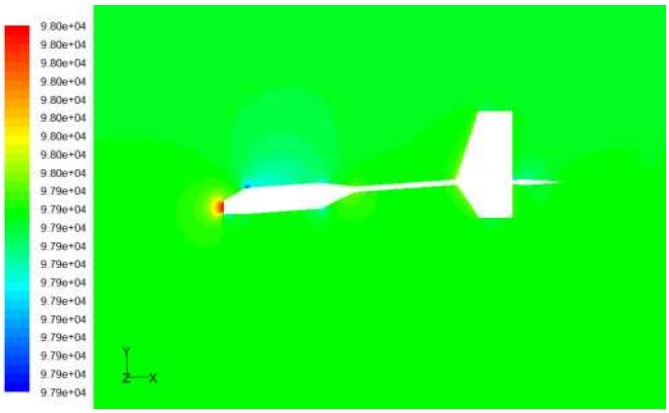

Fig. 4-8 pressure distribution at 4° angle of attack

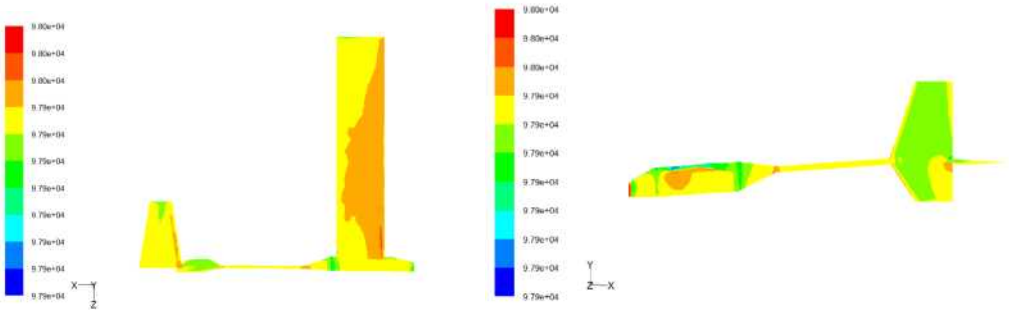

(a) (b)

Fig. 4-9 pressure distribution of the plane surface at 8° angle of attack

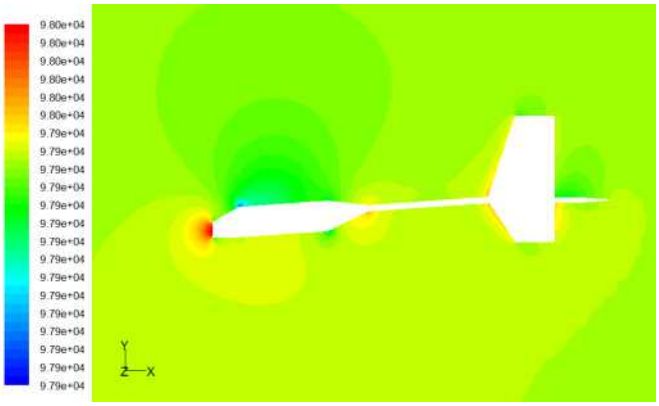

Fig. 4-10 pressure distribution at 12° angle of attack

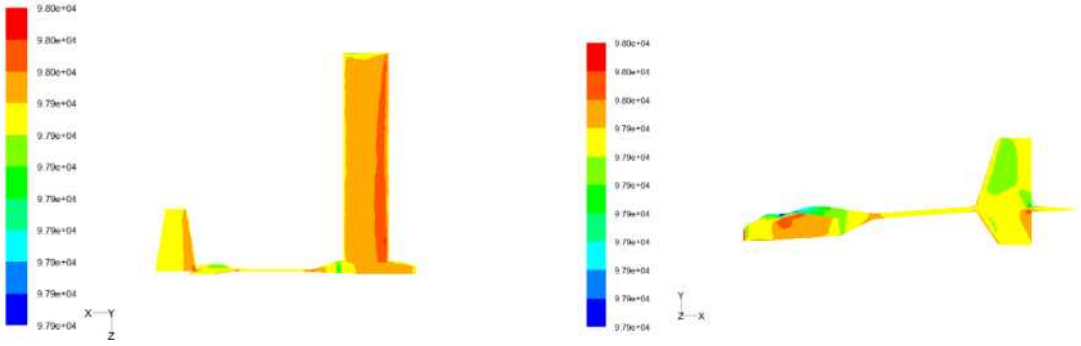

(a) (b)

Fig. 4-11 pressure distribution of the plane surface at 12° angle of attack

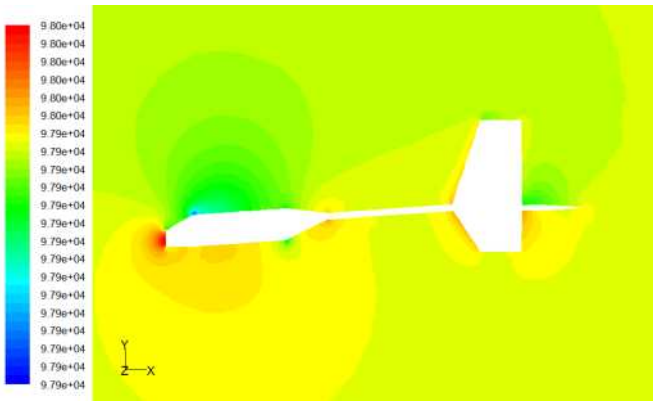

Fig. 4-12 pressure distribution at 12° angle of attack

From Figure 4-3 and 4-12, we can see that the pressure distribution is connected with the angle of attack, but did not change a lot in general. With the increase of the angle of attack, the pressure of the surface area decreases, and the minimum pressure point on the surface move forward. Changes of the bottom of the aircraft are on the

contrary, with increasing angle of attack, the minimum pressure point of the bottom moves backwards with the increase of the angle of attack.

4.3.2 Oil flow distribution

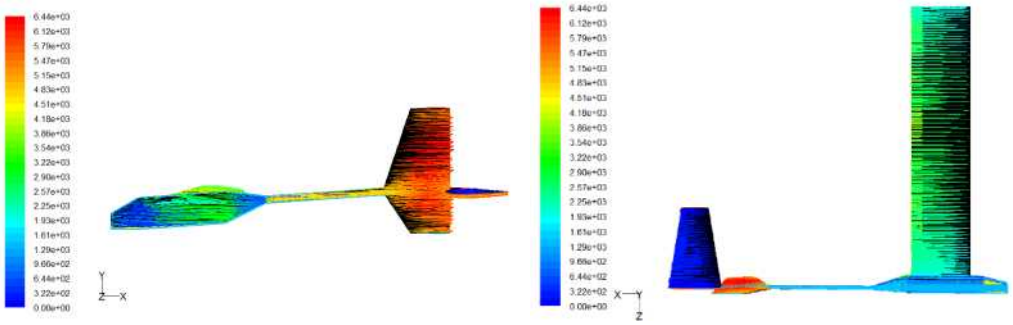

(a) (b)

Fig. 4-13 oil flow distribution at 0° angle of attack

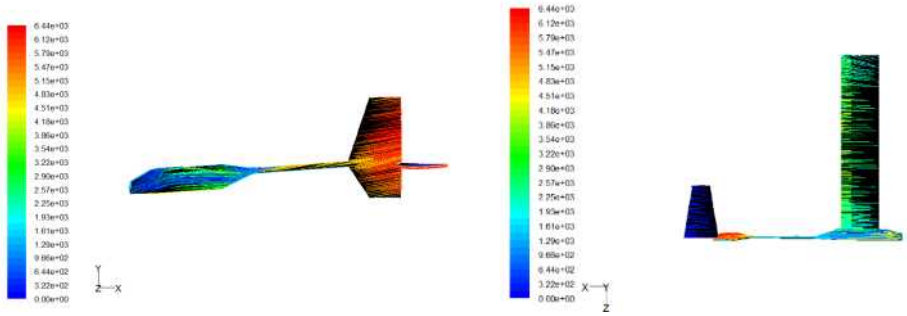

(a) (b)

Fig. 4-14 oil flow distribution at 12° angle of attack

Compare figure 4-13 and figure 4-14. It was found that when the aircraft angle of attack change from 0 degree to 12 degree, because of the low aircraft flight speed, the pressure gradient doesn't change a lot, and obvious eddies are not observed.

4.3.3 Velocity vector distribution

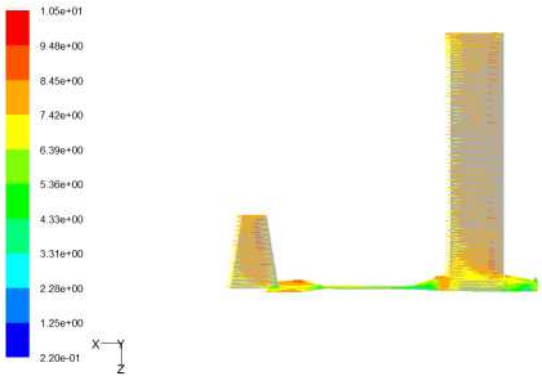

Fig. 4-15 velocity vector distribution at 0° angle of attack

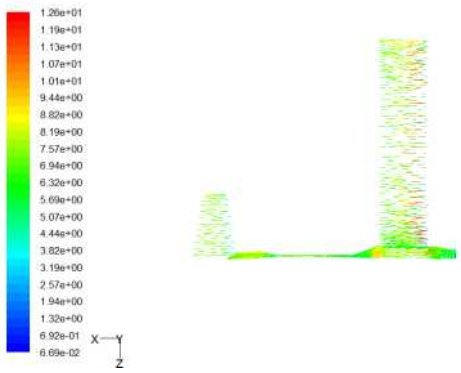

Fig. 4-16 velocity vector distribution at 12° angle of attack

Table 4-1 provides the lift, drag, pitching moment under different angle of attack.

Tab. 4-1 lift, drag, pitching moment under different angle of attack.

angle of attack/°	lift/N	drag/N	Pitching moment/N·m
-4	9.174093	3.340372	11.81636
-2	27.55807	2.266681	6.633171
0	45.93012	1.849135	1.404054
2	66.80744	2.624578	-3.95628
4	77.54435	3.793708	-9.19196
6	100.8077	5.010558	-14.467
8	113.3341	6.573375	-19.7158
10	137.5517	8.517949	-24.899
12	143.1588	11.16639	-30.2331

From the equations below:

$$C_L = \frac{L}{\frac{1}{2}\rho S V^2} \tag{4-1}$$

$$C_D = \frac{D}{\frac{1}{2}\rho S V^2} \tag{4-2}$$

$$C_M = \frac{M_Z}{\frac{1}{2}\rho S V^2 l} \tag{4-3}$$

We can calculate the lift coefficientC_L, drag coefficientC_D, and pitching moment C_M, and get the corresponding curves.

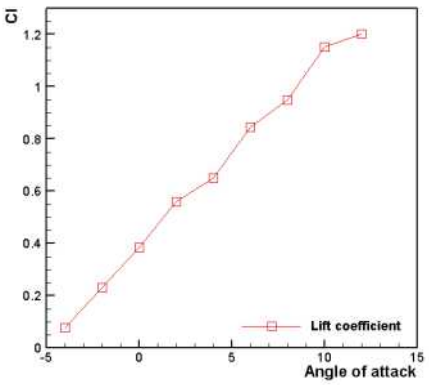

Fig. 4-17 lift coefficient curve

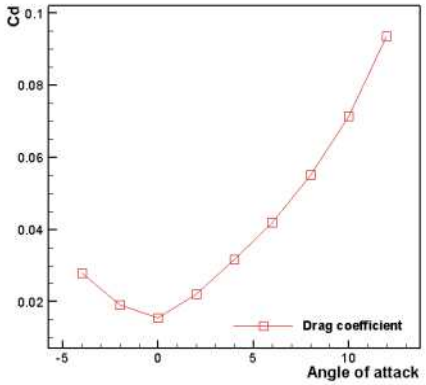

Fig. 4-18 drag coefficient curve

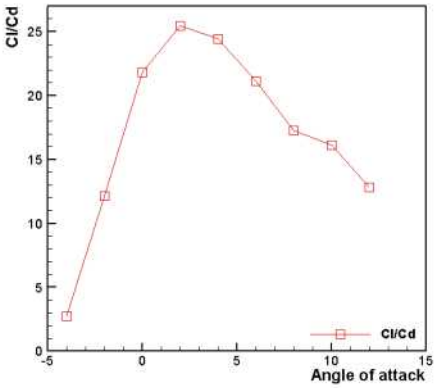

Fig. 4-19 lift-drag ratio curve

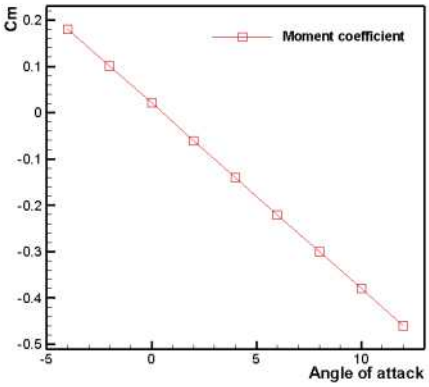

Fig. 4-20 pitching moment curve

It can be seen from the above diagrams that the lift increases with the increase of the angle of attack, which is basically linear. When the angle of attack is large than

10 °, the lift coefficient curve slope became smaller; When the Angle of attack is negative, the resistance decreases with the decrease of the absolute value of the angle of attack, and then when the angle is greater than 0 °, resistance increases with the increase of the angle of attack, the least resistance is reached when the angle is 0 °. Before 4 °, aircraft lift-to-drag ratio increases with the increase of the angle of attack, and reach the maximum value near 4 °. After 4 ° it begins a slow declination; Torque decreases with the increase of angle of attack. The pitching moment is minimal at 0° .